CONF-851217--31

ION IMPLANTATION AT ELEVATED TEMPERATURES*

Nghi Q. Lam and Gary K. Leaf
Argonne National Laboratory
Argonne, IL 60439

CONF-851217--31

DE86 005537

FINAL

November 1985

To be presented at the 1985 Materials Research Society (MRS) Fall Meeting, December 2-6, 1985, Boston, MA.
*Work supported by the U. S. Department of Energy, BES-Materials Sciences, and BES-Applied Mathematical Sciences, under Contract W-31-109-Eng-38.

MASTER

ION IMPLANTATION AT ELEVATED TEMPERATURES*

Nghi Q. Lam and Gary K. Leaf
Argonne National Laboratory
Argonne, IL 60439

FINAL

November 1985

To be presented at the 1985 Materials Research Society (MRS) Fall Meeting, December 2-6, 1985, Boston, MA.
*Work supported by the U. S. Department of Energy, BES-Materials Sciences, and BES-Applied Mathematical Sciences, under Contract W-31-109-Eng-38.

ION IMPLANTATION AT ELEVATED TEMPERATURES*

NGHI Q. LAM and GARY K. LEAF
Argonne National Laboratory, 9700 S. Cass Ave., Argonne, IL 60439

ABSTRACT

A kinetic model has been developed to investigate the synergistic effects of radiation-enhanced diffusion, radiation-induced segregation and preferential sputtering on the spatial redistribution of implanted solutes during implantation at elevated temperatures. Sample calculations were performed for Al^+ and Si^+ ions implanted into Ni. With the present model, the influence of various implantation parameters on the evolution of implant concentration profiles could be examined in details.

INTRODUCTION

During ion implantation, nonequilibrium point defects are produced in large numbers by the violent slowing-down of energetic ions in the host matrix. Spatial nonuniformity in the defect production and annihilation gives rise to persistent defect fluxes, e.g., towards the surface, or from the peak-damage region towards the mid-range and beyond-range regions where the defect-production rates are significantly lower. At elevated temperatures, these defect fluxes can preferentially transport certain alloying elements via defect-solute interactions, which causes a spatial redistribution of implanted species. This nonequilibrium phenomenon, called radiation-induced segregation (RIS), acts ynergistically with radiation-enhanced diffusion (RED) and preferential sputtering (PS) during ion implantation, introducing a great complexity to the understanding of this process.

A comprehensive kinetic model has been developed recently to investigate the synergistic effects of all the processes mentioned above on the spatial redistribution of implanted atoms during implantation. The effects of spatially-nonuniform rates of damage and ion deposition, as well as the movement of the bombarded surface as a result of sputtering and introduction of foreign atoms into the system, were taken into account. The evolution of implant concentration profile in time and space was calculated for various temperatures, ion energies, and ion-target combinations. The results of the present work may be useful in elucidating the essential physics of the elevated-temperature ion implantation process.

BASIC KINETICS

We consider a metal substrate B into which A atoms are implanted at a flux ϕ (ions/cm^2·s). A number of A atoms will end up in interstitial sites, and the rest in substitutional sites of the host lattice. The respective rates of implantation into these sites are $f_i\phi$ and $f_s\phi$ (atom fraction/s). During implantation, point defects - vacancies and interstitials - are created by ion impact at a rate K (displacements per atom per second, dpa/s). Since the interstitial defects are distinguishable, the rate of interstitial production is partitioned into KC_{sA} and $KC_{sB} \equiv K(1-C_{sA})$ for A- and B-interstitials, respectively, with C_{sA} and C_{sB} being the respective concentrations of A and B atoms in substitution. The interstitials and vacancies annihilate by mutual recombination and/or diffusion to defect

*Work supported by the U. S. Department of Energy, BES-Materials Sciences, and BES-Applied Mathematical Sciences, under Contract W-31-109-Eng-38.

sinks. In addition, vacancies and B-interstitials can interact with free solute atoms, giving rise to the formation of vacancy-solute complexes and conversion of B-interstitials to A-interstitials, respectively.

The local concentrations (in atomic fractions) of vacancies (v), B-interstitials (iB), A-interstitials (iA), A-vacancy complexes (vA) and free substitutional solutes (sA) change with implantation time according to the following system of kinetic equations:

$$\begin{aligned}
\frac{\partial C_v}{\partial t} &= -\nabla\cdot J_v + K - f_s\phi + F_v \\
\frac{\partial C_{iB}}{\partial t} &= -\nabla\cdot J_{iB} + K(1-C_{sA}) + F_{iB} \\
\frac{\partial C_{iA}}{\partial t} &= -\nabla\cdot J_{iA} + KC_{sA} + f_i\phi + F_{iA} \\
\frac{\partial C_{vA}}{\partial t} &= -\nabla\cdot J_{vA} + F_{vA} \\
\frac{\partial C_{sA}}{\partial t} &= -\nabla\cdot J_{sA} - KC_{sA} + f_s\phi + F_{sA}
\end{aligned} \qquad (1)$$

where the F's denote the local rates of creation and loss of species by chemical-type reactions (i.e. formation and dissociation of defect-solute complexes, and defect recombination and annihilation), and the J's are the fluxes of the mobile species, defined as [1]:

$$J_v = -(1 + \sigma_v C_{sA})D_v \nabla C_v \qquad (2a)$$

$$J_{iB} = -(1 + \sigma_i C_{sA})D_{iB} \nabla C_{iB} \qquad (2b)$$

$$J_{iA} = -D_{iA} \nabla C_{iA} \qquad (2c)$$

$$J_{vA} = -D_{vA} \nabla C_{vA} \qquad (2d)$$

$$J_{sA} = -\sigma_i C_{sA} D_{iB} \nabla C_{iB} + \sigma_v C_{sA} D_v \nabla C_v \ . \qquad (2e)$$

Here, the fluxes of defects and defect-solute complexes are proportional to their concentration gradients, the proportionality constants being the diffusion coefficients D_v, D_{iB}, D_{iA} and D_{vA}. The constants σ_v and σ_i are the capture factors for vacancy-solute and interstitial-solute encounters [1,2]. For strong defect-solute binding, $\sigma_v = 6$ and $\sigma_i = 6$, and for repulsion or no interaction, $\sigma_v = 2$ and $\sigma_i = 0$. The free solute flux arises from the coupling of A atoms with free B-interstitial and vacancy fluxes. Note that the vacancy flux-induced solute current, which is the last term of equation (2e), has the opposite sign of the other terms, because atom transport occurs in the direction opposite to that of the vacancy flux. The reader is referred to ref. [3] for more details of the model.

Concurrently with the buildup of solute concentration in the host matrix, the surface is subjected to displacements, due to the introduction of foreign atoms into the system and sputtering. The former gives rise to surface relaxation in the - x direction, at a rate $\dot{\delta}_-$, whereas the latter causes surface recession in the + x direction, at a rate $\dot{\delta}_+$. The rate $\dot{\delta}_-$ can be calculated from the net atom flux towards the surface:

$$\dot{\delta}_- = J_{iA} + J_{iB} - J_v - J_{vA} \ , \qquad (3)$$

while the rate $\dot{\delta}_+$ is determined by the ion flux, the partial sputtering coefficients, S_A and S_B, and the surface concentrations of A and B atoms:

$$\dot{\delta}_+ = \phi\Omega[S_A C_A^s + S_B(1 - C_A^s)] \ , \qquad (4)$$

where Ω is the average atomic volume. The net surface displacement rate,

$$\dot{\delta} \equiv \frac{d\delta}{dt} = \dot{\delta}_- + \dot{\delta}_+ \qquad (5)$$

is therefore controlled by the competition between the rates of ion collection and sputtering.

Equations (1) and (5) were solved numerically for a semi-infinite medium with the aid of the LSODE package of subroutines [4], starting from the thermodynamic equilibrium conditions. A moving boundary, which represents the receding surface, was accommodated by a transformation of the physical space x to a reduced space z:

$$z = 1 - \exp[-\beta(x - \delta)] \qquad (6)$$

where β is a scaling factor. With this transformation, the region $\delta \leq x < \infty$ was mapped into the fixed region $0 \leq z < 1$.

Sample calculations were performed for two model systems: Al^+ and Si^+ implantations into Ni. The physical parameters used were tabulated in ref. [3]. The ions were implanted at 50 and 400 keV. The spatial dependence of the rates of defect production and ion deposition was calculated using the TRIM code [5], with a displacement energy of 30 eV. The most-probable damage and ion ranges for 50-keV Al^+ and Si^+ in Ni are ~13 and 27 nm, and ~12 and 24 nm, respectively. For 400-keV Al^+ and Si^+ in Ni, the respective most-probable ranges are ~175 and 235 nm, and ~160 and 215 nm. At 50 keV, sputtering is significant; the sputtering coefficients for the host and solute atoms, S_B and S_A, in Ni-Al and Ni-Si alloys were taken to be 3.5 and 2.0 atoms/ion, and 3.5 and 1.0 atoms/ion, respectively [6]. Here, we assumed that S_A and S_B were equal to the coefficients for the respective pure A and B elements. At 400 keV, sputtering is significantly reduced [6]; it was, however, assumed to be negligible in the present calculations. For each ion-target combination, the defect-production rate K was taken as $0.3K_o$, where K_o is the calculated rate of defect production, and the factor 0.3 is the defect-production efficiency [7].

SAMPLE CALCULATIONS

Time and temperature dependence of implant redistribution during high-energy implantation

The time evolution of the Al redistribution during 400-keV implantation at 100, 500 and 800°C is shown in Fig. 1. The ion flux was 6.25×10^{13} ions/cm^2·s and the corresponding peak-damage rate was calculated to be $K_o^{max} = 4.92 \times 10^{-2}$ dpa/s. The most-probable damage and ion ranges are marked by R_d and R_i. The dislocation density was assumed to remain constant at 10^6 disl/cm^2 throughout the target during implantation. Since sputtering was assumed to be negligible, the surface relaxed in the - x direction; the calculated surface displacements, δ, are indicated in the figure for various times. During implantation, under the influence of damage-rate gradients, point defects flow out of the peak-damage region towards the surface and into the beyond-range region. Since Al solutes segregate in the direction opposite to the defect fluxes in irradiated Ni, there exists a net flux of Al atoms into the peak-damage region [8]. Consequently, there is no shift of the implant profile towards the sample interior; the ion distribution simply broadens with time. The effect of RIS on the implant distribution can also be demonstrated by the near-surface Al depletion on high-dose profiles, especially around 500°C where Al depletion is most severe. Long tails extending deep into the bulk, resulting from RED of Al atoms from the ion-peak region, are observed on the solute profiles for $t > 10^2$s. The contribution of RIS to the evolution of the Al tails is unimportant, because Al atoms and point defects migrate in opposite directions. The temperature dependence of the penetration

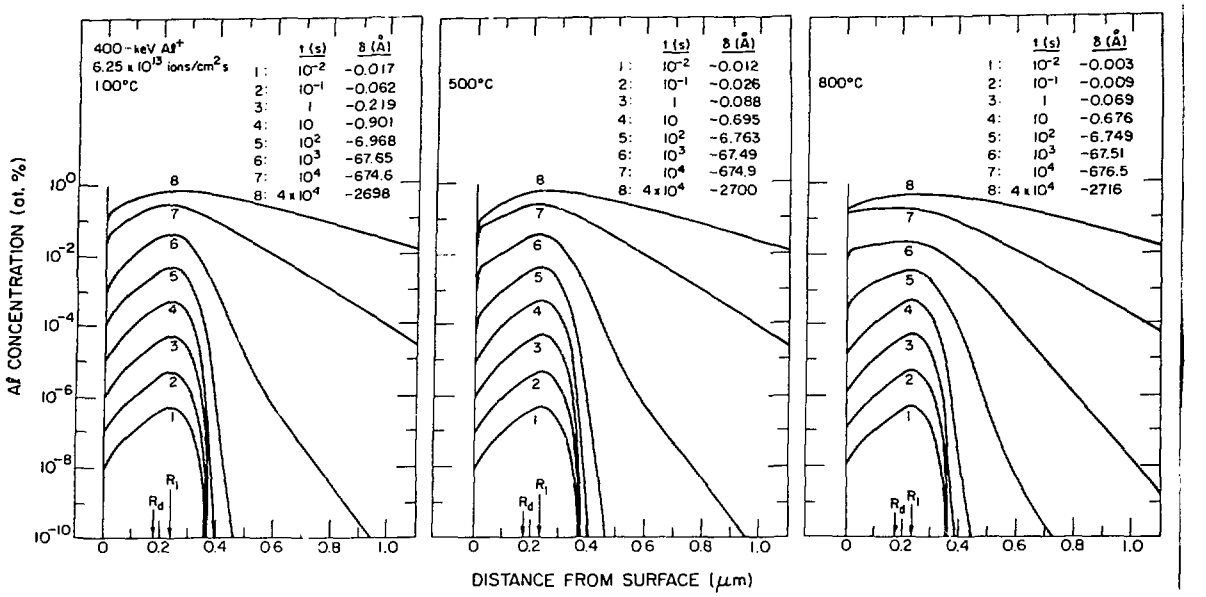

Fig. 1. Time evolution of the Al concentration profiles during 400-keV implantation at 100, 500 and 800°C.

tails is, however, rather weak, because Al transport occurs via the dominant interstitialcy mechanism. It should be pointed out that RED is efficient during implantation because the effective rate of interstitial production is always larger than the vacancy-production rate.

Figure 2 illustrates the time dependence of the Si redistribution during implantation at 100, 500 and 900°C. The calculated peak-damage rate was $K_o^{max} = 5.6 \times 10^{-2}$ dpa/s. The values of δ are indicated in the

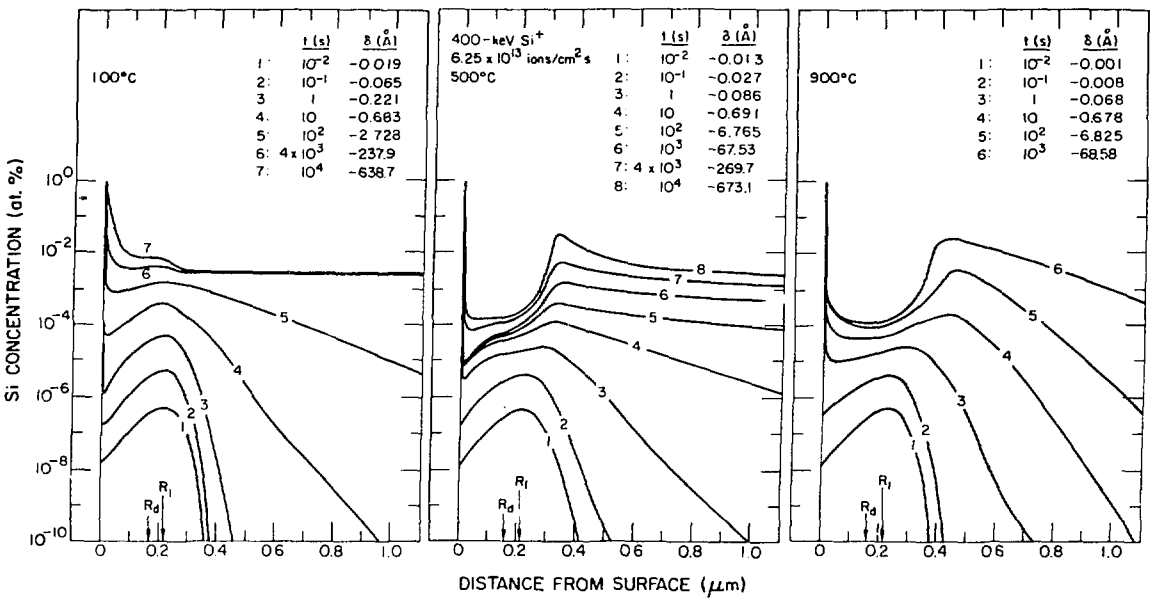

Fig. 2. Time evolution of the Si concentration profiles during 400-keV implantation at 100, 500 and 900°C.

figure. During implantation at elevated temperatures, the preferential association between Si atoms and Ni-interstitials induces a net flux of Si in the same direction as the defect fluxes, out of the peak-damage region [8,9]. As a result, after a short implantation time at, e.g., 500°C, a

depression in the Si concentration occurs in the peak-damage region, and a pronounced increase is seen at the surface and in the beyond-range region. The implant distribution peak moves inward, and eventually stops at a position near the end of the ion range. Unlike the Al-implantation case, the penetration tails on the Si profiles are caused by a combination of RIS and RED via an interstitialcy mechanism. For a given temperature and dose, these tails are significantly higher and longer than those on the Al concentration profiles shown in Fig. 1. At 100°C, the Si distribution peak is not shifted, only solute enrichment at the surface and long tails are observed. The tails on the 100 and 900°C profiles are, however, shorter than those at intermediate temperatures, e.g. 500°C, because of the decrease in the effectiveness of RIS at low ($\lesssim 0.2T_m$) and high ($\gtrsim 0.7T_m$) temperatures. The predicted shift of the Si distribution peak into the bulk is consistent with recent experimental measurements by Mayer et al. [10] in Si-implanted Ni at elevated temperatures.

Effect of preferential sputtering on implant distribution during low-energy implantation

Redistributions of Al and Si solutes in Ni during 50-keV implantation at 500°C are presented in Figs. 3 and 4, respectively. The rates of defect production and ion deposition, normalized to their peak values, are included in the top portions. For the ion flux used, 6.25×10^{13} ions/cm^2·s, the calculated peak-damage rates were $K_o^{max} = 7.92 \times 10^{-2}$ and 8.63×10^{-2} dpa/s for Al^+ and Si^+ bombardments of Ni, respectively. Since sputtering is significant at this energy, the bombarded surface recedes into the sample with time. The surface displacements are indicated in the figures.

In the Al-implantation case (Fig. 3), the Al concentration at the surface, C_{Al}^s, increases with time to a quasi-steady-state value, which is mainly determined by the sputtering coefficients and the sub-surface implant concentration. The time required to achieve quasi-steady-state is $\sim 10^4$s. The quasi-steady-state value of C_{Al}^s, 45.9 at.%, is significantly larger than that obtained in the high-energy implantation case, where C_{Al}^s is controlled by RIS. The total implant concentration remaining in the substrate is, however, smaller due to sputtering. The quasi-steady-state implant profile does not resemble the high-energy implantation profile (compare with Fig. 1); it decreases monotonically with depth from the value of C_{Al}^s.

The temporal evolution of the Si profile (Fig. 4) is quite different from that for Al, due to the different RIS behaviors. After a short time, e.g. 0.1 s, Si enrichment occurs at the surface, because of RIS and relatively small ion range, and the Si distribution peak starts moving into the sample interior. However, as the implantation goes on, the Si concentration at the surface, C_{Si}^s, decreases with time and eventually attains a quasi-steady-state value of $\sim 3.8 \times 10^{-4}$ at.% for $t > 10^4$s. This value is five-orders-of-magnitude smaller than C_{Al}^s, because, in this case, most of the implanted Si atoms segregate into the bulk. The Si profile always changes with time, even though C_{Si}^s does attain its quasi-steady-state value. The implant distribution continuously shifts towards the interior, and high-level tails extending deep into the sample are observed behind the distribution peak for $T \gtrsim 10^3$s.

ACKNOWLEDGEMENTS

The authors have greatly benefited from useful discussions with Prof. R. A. Johnson and Dr. H. Wiedersich. Mrs. Diane Livengood's contributions in skillfully formatting and typing the paper are also gratefully acknowledged.

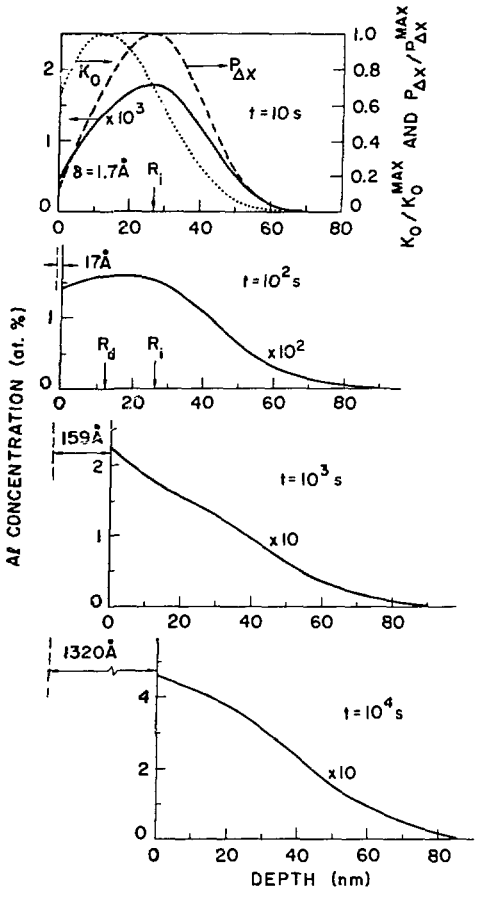

Fig. 3

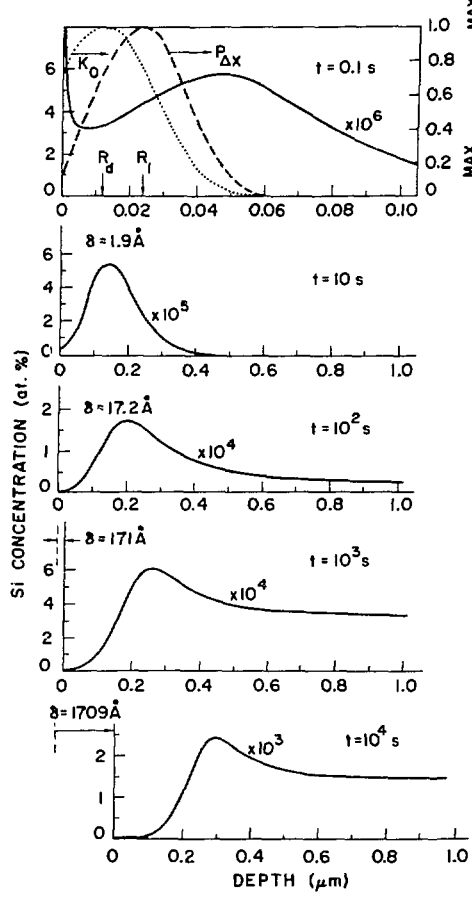

Fig. 4

Fig. 3. Development of the Al profiles during 50-keV implantation at 500°C. The normalized damage (K_0) and ion-deposition ($P_{\Delta x}$) rates are included in the top portion. The surface displacements, δ, resulting from sputtering are indicated.

Fig. 4. Development of the Si profiles during 50-keV implantation at 500°C. The normalized damage and ion-deposition rates are shown in the top portion. Note that the depth scales in plots for t = 0.1 s and t ≥ 10 s differ by a factor of 10.

REFERENCES

1. R. A. Johnson and N. Q. Lam, Phys. Rev. B13, 4364 (1976).
2. A. Barbu, Acta Metall. 28, 499 (1980).
3. N. Q. Lam and G. K. Leaf, submitted to J. Mater. Res.
4. A. C. Hindmarsh, in: Scientific Computing, eds. R. S. Stepleman et al. (North-Holland, Amsterdam, 1983) p. 55.
5. J. P. Biersack and L. G. Haggmark, Nucl. Instr. Methods 174, 257 (1980).
6. H. H. Andersen and H. L. Bay, in Sputtering by Particle Bombardment, ed. R. Behrisch (Springer, Heidelberg, 1981) p. 145.
7. P. R. Okamoto, L. E. Rehn and R. S. Averback, J. Nucl. Mater. 133 & 134, 373 (1985).
8. N. Q. Lam, P. R. Okamoto and R. A. Johnson, J. Nucl. Mater. 74, 101 (1978).
9. N. Q. Lam, K. Janghorban and A. J. Ardell, J. Nucl. Mater. 101, 314 (1981).
10. S. G. B. Mayer, F. F. Milillo and D. I. Potter, Mat. Res. Soc. Symp. Proc. 39, 521 (1985).